16th World Conference on Earthquake Engineering, 16WCEE 2017
Santiago Chile, January 9th to 13th 2017
Paper N° 1741
Registration Code: S-S1463246460

# IMAGE ANALYSIS METHOD FOR OBSERVING CRACK, STRAIN AND DISPLACEMENT FIELDS IN RC STRUCTURAL EXPERIMENTS

Y. S. Yang [(1)], J. E. Woods [(2)], and D. T. Lau[(3)]

[(1)] *Associate Professor, National Taipei University of Technology, Dept. of Civil Eng., Taipei, Taiwan, ysyang@ntut.edu.tw*
[(2)] *Graduate Student, Carleton University, Dept. of Civil and Env. Eng., Ottawa, Canada, josh.woods@carleton.ca*
[(3)]*Professor, Carleton University, Dept. of Civil and Env. Eng., Ottawa, Canada, david.lau@carleton.ca*

## Abstract

This paper presents an image analysis method that is capable of capturing crack distributions, displacement and strain fields in structural testing of reinforced concrete (RC) elements. Traditionally, crack distributions are recorded by manually marking visible cracks in the concrete during an experiment. Strain profiles and displacements of the test specimen are recorded using strain and displacement gauges located at specific measurement locations on the test specimen. The use of such techniques can be time consuming and expensive, requiring significant investment in the cost of the sensors, time for their installation, and large data acquisition systems to collect the data. The use of such measurement systems also requires a priori knowledge of specific measurement locations, something that may not be obvious for large scale experimental testing. Alternatively, the image analysis technique presented herein is a freely available software tool, ImPro Stereo. ImPro Stereo provides a cost effective reliable measurement tool capable of capturing crack progressions, surface strain fields, and displacement time histories in a large-scale structural experiment. To validate the performance of the image analysis method, it is implemented in an experimental program on the in-plane seismic behavior of RC shear walls rehabilitated using fiber-reinforced polymer (FRP) sheets. The image analysis method is shown to be capable of measuring crack distributions and displacement fields over the entire surface of the shear wall with a high degree of accuracy. Strain profiles can be estimated according to the surface displacements. Experimental results from the image analysis method are utilized to develop a better understanding of the behaviour of RC shear walls retrofitted with FRP sheets for earthquake resistance. Potential field applications for the image analysis method in FRP-strengthened RC structures are also discussed.

*Keywords: reinforced concrete; shear wall; cyclic test; fiber-reinforced polymer; image analysis; ImPro Stereo*

## 1. Introduction

In earthquake engineering, the behaviour of structural elements under the forces and displacement induced by seismic ground motions can be difficult to predict using analytical tools alone. Experimental testing plays a key role in providing information on the behaviour of structural components and forms the basis for the development of design equations and the adaptation of such equations in design standards around the world. The development of different testing schemes, including quasi-static cyclic loading and hybrid simulation has allowed engineers to get a better understanding of the behaviour of structural elements and systems under earthquake loading. During experimental testing, measurement of displacements and strains of the test specimen play an important role in understanding the behaviour of the element beyond what is visible by the naked eye. In reinforced concrete (RC) elements, the formations of cracks in the concrete in addition to displacements and strains can help to quantify the behavior of the component and identify different modes of failure. In recent years, the use of advanced composite materials, such as fiber-reinforced polymer (FRP) sheets has become an acceptable solution to improve the performance of RC elements under earthquake loading. A number of researchers have studied the use of externally bonded FRP sheets to strengthen RC beams, slabs, walls and columns. In tests on RC elements strengthened with externally bonded FRP sheets, separation between the FRP laminate and the concrete substrate is often observed and is a phenomenon referred to as FRP debonding, as illustrated in Fig. 1a. Tracking the progression of FRP debonding patterns in FRP retrofitted RC members is a crucial component in establishing a detailed understanding of the behavioral mechanisms of the concrete and FRP sheets.

Traditionally, strains and displacements in structural experiments are measured using electrical strain and displacement gauges located at critical locations on the test specimen. Although these gauges are effective in capturing the response parameters, the critical locations for these devices may not always be obvious, especially in large scale structural tests. When a large number of sensors are required, the installation and setup time for the sensors can be tedious and costly. As shown in Fig. 1b, crack distributions in RC elements are typically measured manually by stopping the experiment and outlining the visible cracks in the concrete using a pen or marker. Furthermore, the traditional technique to monitor debonding between the FRP sheets and RC surface is to use a rubber hammer and listen for a change in sound when striking the FRP sheet. A hollow sound indicates that the FRP sheet has separated from the concrete. In such cases, the measurement of crack distributions and FRP debonding progressions are time consuming and potentially dangerous; when the structural element is left under load so that workers can approach to study the specimen. Furthermore, testing of elements under earthquake loading often requires the load to be applied continuously without stopping to prevent relaxation of the test specimen, making it difficult to take detailed measurements such as crack widths during testing.

This paper presents an image analysis method capable of measuring displacement and strain fields in addition to identifying cracks over the entire surface of a structural element. This paper will use an image

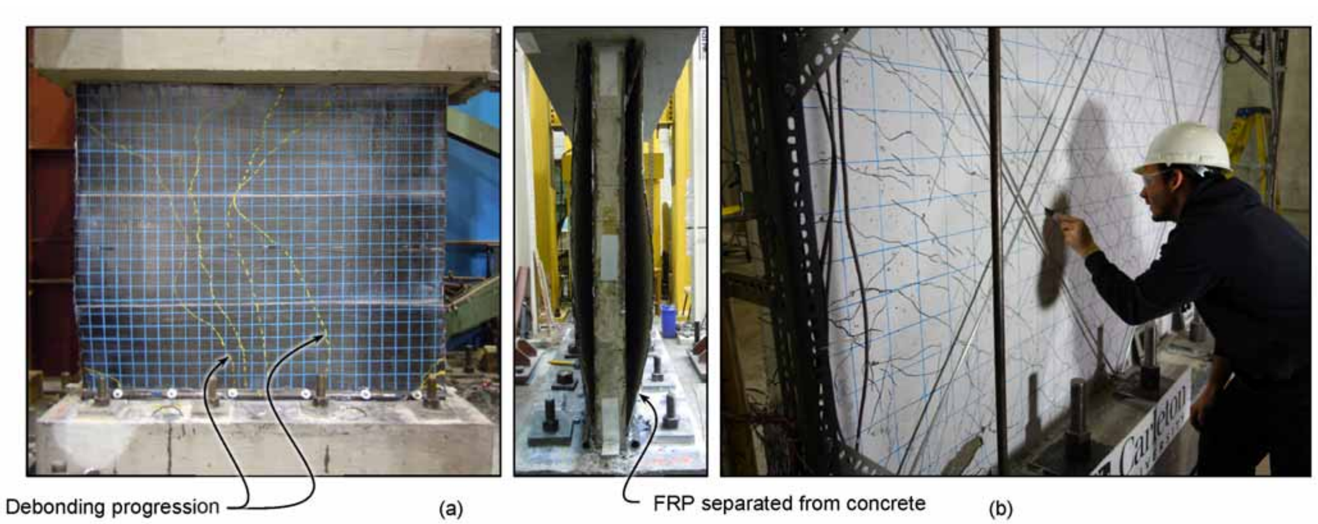


Fig. 1 – (a) Typical FRP-concrete debonding; (b) Traditional concrete crack marking procedure

analysis method to attempt to detect debonding between the FRP sheets and the concrete substrate. The technique uses high-definition photographs taken at various stages throughout the experiment. The images are processed using a freely available software tool called ImPro Stereo [1]. Using ImPro Stereo, photos of the damaged specimen are compared to the baseline photos taken at the beginning of the test to determine the displacement and strain fields over a specific area of interest on the surface of the test specimen. Past studies have employed this image analysis technique to monitor crack widths and measure strain and displacement fields in structural experiments on a RC wall and the tubular surface of a RC column [2, 3]. However, in both of these studies the monitored measurement region represented a small section of the total surface of the structural element. In this study, the image analysis method is employed to capture the in-plane displacement and strain distribution over the entire face of the RC specimen. The test specimens are deficient RC shear walls designed according to older design standards. The specimens are tested under in-plane cyclic lateral load to simulate the drift and damage effects of an earthquake. To improve the seismic performance of the walls, FRP sheets are applied to the surfaces of the specimens. Results of the test will allow for comparison of displacement and strain fields between the plain RC walls and the FRP retrofitted walls. Results will also determine if the ImPro Stereo technique is capable of identifying if the FRP sheet separates/debonds from the concrete substrate during testing.

## 2. Image Analysis Technique

The image analysis tool presented herein provides a simple, safe, cost effective method for measuring in-plane displacement and strain fields in addition to monitoring crack widths in structural experiments on RC elements. The method uses a tool named ImPro Stereo to analyze the photos. The software is freely available, and uses a MATLAB based program, Bouguets Camera Calibration Toolbox and OpenCV library [4, 5]. Before the experiment is conducted, there are preliminary steps that must be completed to ensure that the results of the image-based analysis are accurate. These steps include preparing the surface of the test specimen, mounting the two cameras and taking calibration photos. Surface preparation consists of painting or marking the surface of the test specimen to ensure that the measurement region, referred to as the region of interest (ROI), has enough unique characteristics to detect movement. The common method for surface preparation and the method used in this experimental program is a speckle pattern technique, which applies tiny speckles over the entire ROI. These speckles form unique identifiers that can be used to track the movement in the ROI during loading. Figure 2 shows the outline of a typical ROI and the speckle pattern on the surface of the wall.

After applying the speckle pattern to the surface of the specimen, the cameras are set in place next to one another and focused on the ROI, as shown in Fig. 2. Using this image analysis method, the cameras are not required to be placed directly perpendicular to the ROI, but should be positioned such that the ROI is located within the centre portion of the camera view. This will ensure the ROI remains within the camera view

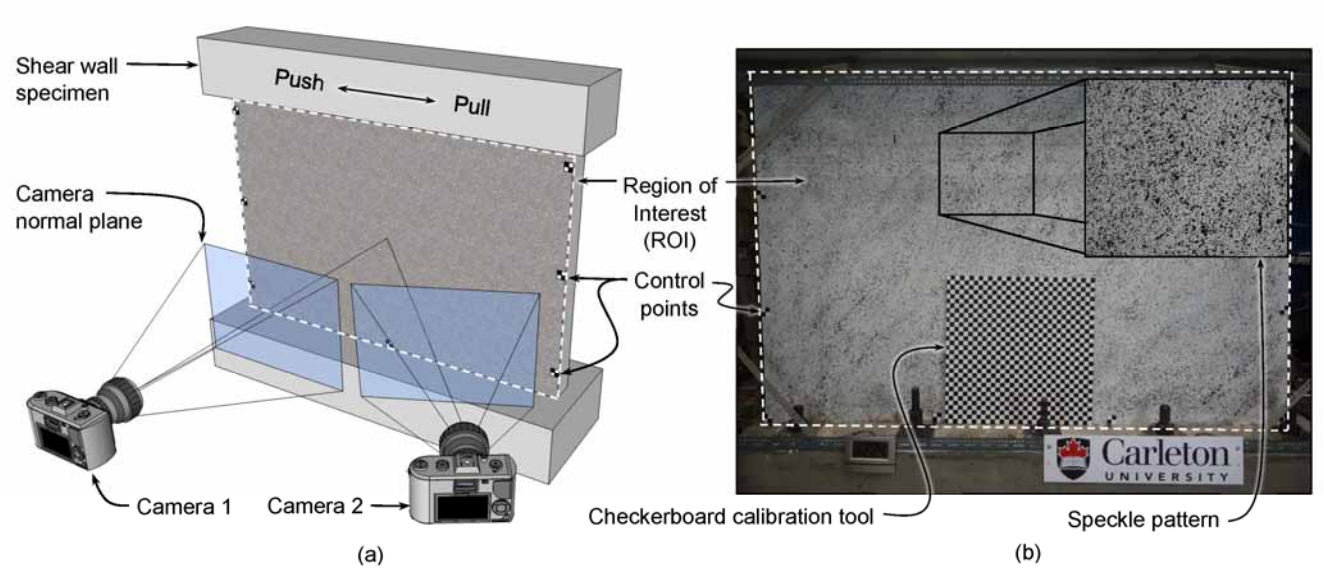


Fig. 2 – Typical test setup for the image-analysis method

throughout the entire test and the higher distortion effects close to the edges of the camera view can be avoided. Throughout the duration of the test, the cameras should remain fixed, avoiding any slight movements, which would decrease the accuracy of the measurement system. Prior to testing, pairs of calibration photos are used to provide information on each camera in addition to the position of each camera relative to the ROI and relative to one another. An object with a checkerboard pattern (Fig. 2) is placed in the ROI during the calibration photos. Because the ROI in this study is very large, a series of 12 calibration photos are taken with the checkerboard located in different positions around the ROI. Once the test begins, photos are taken incrementally over the course of the experiment. As discussed previously, it is important that the cameras remain firmly fixed throughout the test and that the photos from both cameras are taken simultaneously to ensure the cameras are capturing the state of the specimen at the same instant. A remote connected to both cameras ensures both photos are taken simultaneously and a clock within the ROI is used to match the test photos with other measured parameters (eg. load, displacement, etc…). It is also important to ensure that the apertures, exposure time, lighting conditions, and focal length remain constant throughout the test to avoid distorting the results.

Once the preliminary steps are complete and the photos of the specimen during the test are collected, the images are analyzed using ImPro stereo. Figure 3 shows the user interface for ImPro Stereo. The steps to image analysis include stereo calibration, control point positioning, metric image rectification, surface displacement analysis and visualization. Stereo calibration is conducted using the previous calibration photos and Bouguets Camera Calibration Toolbox [4]. The purpose of the calibration is to estimate the intrinsic parameters of the cameras (eg. lens focus and distortion factors) in addition to extrinsic parameters including the coordinate transformation between cameras. The calibration parameters of the cameras and a stereo triangulation technique are used to identify the 3D locations of the control points on the surface of the ROI. In this study, three control points are manually selected in the ImPro Stereo user interface for the first set of images to completely define the three axes of the measurement region. In the subsequent photos of the deformed test specimen the control points are automatically located using template matching. The surface of the ROI is then converted to a plane image (2D), removing the effects of perspective and image distortion using a process known as metric rectification. As a result, the displacement and strain fields are determined in the plane of the specimen and not in 3D, by analyzing the rectified images of the deformed specimen relative to the initial photos. However, because out-of-plane deformation of the wall specimen is being restrained, significant out-of-plane displacements and strain are not expected to occur. Each of these steps is carried out for four cyclic tests on large scale squat RC structural walls. Two of the tests are on plain RC walls and the second two tests are on FRP retrofitted RC walls. Results from the image analysis method are used to get a better understanding of the behaviour of deficient squat RC shear walls in addition to evaluating the performance of the retrofitting system.

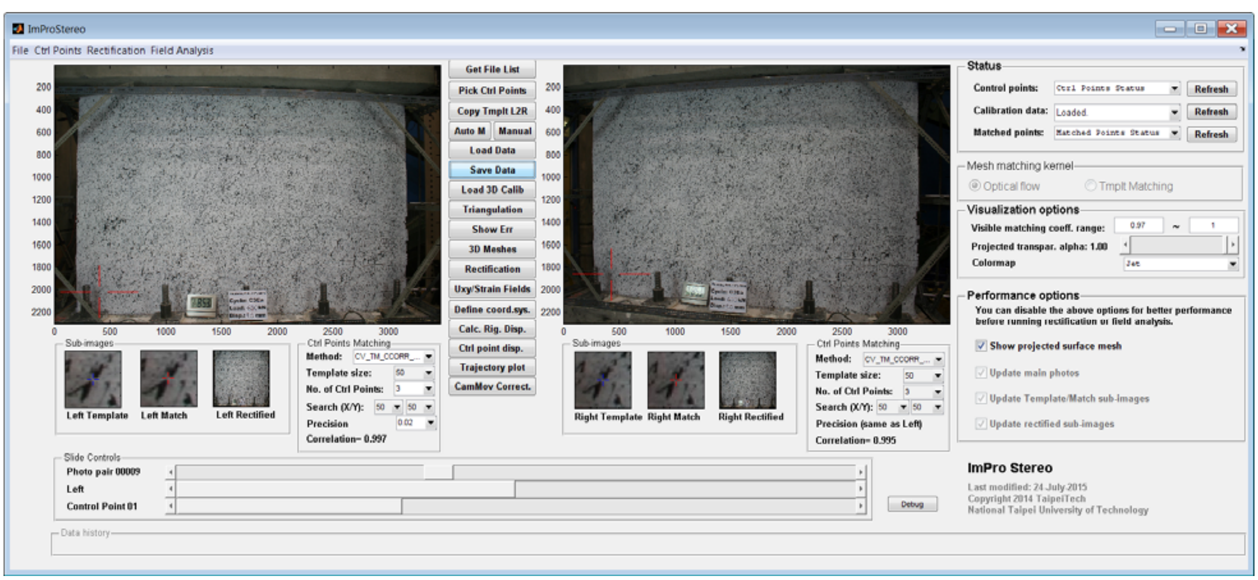


Fig. 3 – ImPro Stereo visual interface and camera calibration

## 3. Shear Wall Experimental Program

The shear wall specimens tested in this study are 2/3 scale cantilevered squat RC shear walls with a height-to-length aspect ratio ($h_w/l_w$) of 0.65, representative of older design standards [6, 7]. As a result, the walls have a number of deficiencies in their design that are shown to lead to poor seismic performance, including insufficient shear reinforcement, no confinement at the two ends of the wall and lap splices of the longitudinal steel reinforcement in the plastic hinge region. The deficiencies in the design of the specimens in combination with the inherent shear dominant nature of low aspect ratio squat walls is expected to lead to a brittle shear dominant response. The goal of the study is to determine the effectiveness of using externally bonded FRP sheets to restore and improve the seismic performance of older squat RC shear walls that have been damaged during an earthquake and must be repaired. A detailed description and results of the experimental program are available in an accompanying paper [8]. The specimens are first tested under cyclic load and are then repaired using externally bonded CFRP sheets. Figure 4 shows a typical test specimen, setup and cyclic lateral load sequence.

Figure 4a shows the dimensions for a typical wall specimen in this study. All four specimens have the same cross sectional details and each specimen is tested twice: once without any additional FRP reinforcement (designated CW1/CW2) and then the same specimens are tested again after applying the externally bonded FRP sheets (designated RW1/RW2). The goal of implementing the image based analysis technique is to demonstrate an accurate, simple, cost-effective method to capture crack development in the plain RC specimens and establish if it is able to capture debonding between the FRP sheets and concrete substrate. Image analysis results will allow for comparison between specimens with and without FRP reinforcement to get a better understanding of the performance of the FRP rehabilitation strategy. Figure 2 shows the 2750 x 1800mm measurement region (ROI) for each specimen, which is painted with a speckled pattern to ensure the surface of the wall has enough unique features to be able to trace movement within the ROI. Two Cannon Rebel XT 8 megapixel cameras are firmly fixed to the laboratory strong floor roughly 1m apart. The shutters of both cameras are simultaneously controlled using a remote. Each camera is set to manual focus, aperture of f/16, and ISO of 100.

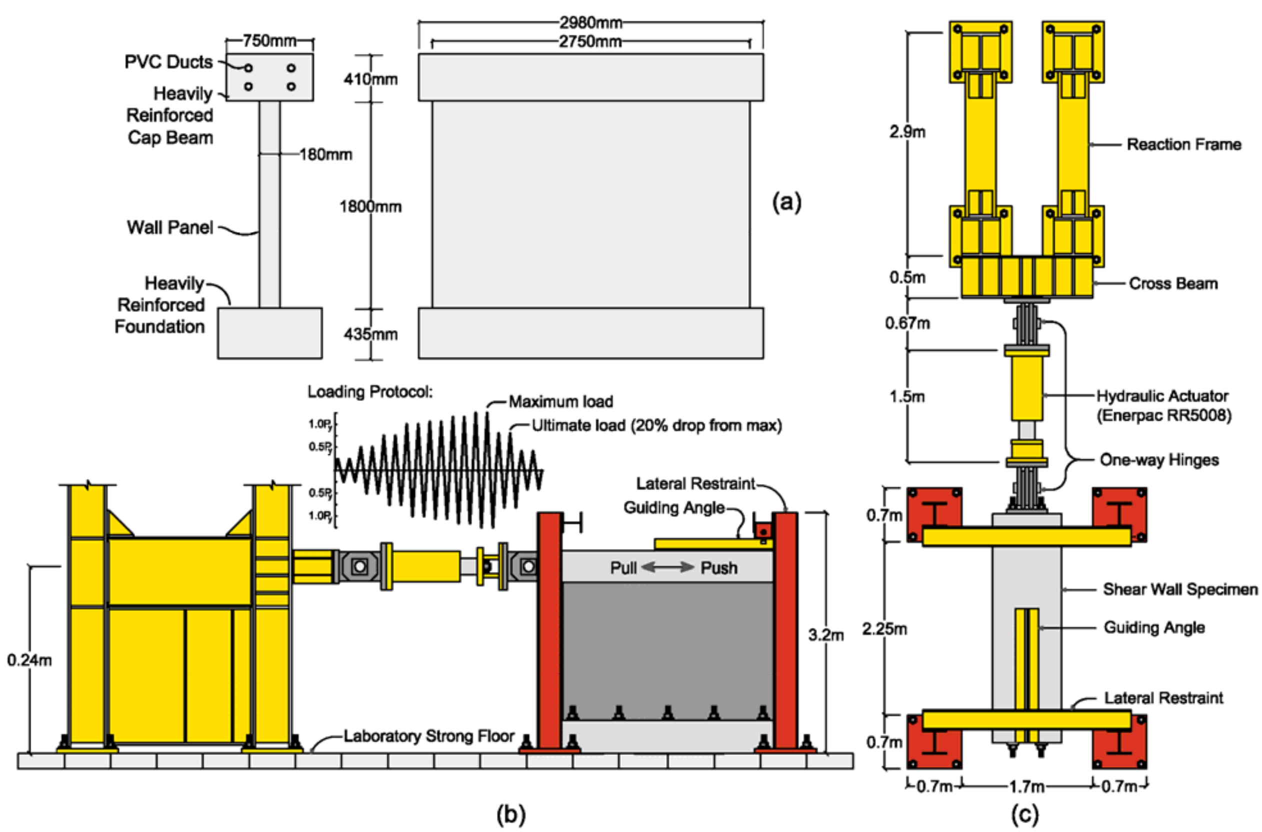


Fig. 4 – (a) Typical shear wall specimen; (b) experimental test setup; (c) top view

## 4. Experimental Results

The surface strain fields and crack distributions for the four test specimens (i.e., CW1, RW1, CW2, RW2) are determined by analyzing hundreds of pairs of images from each test using ImPro Stereo. Due to limitations on space, this paper only presents those taken at the peak of each cycle. Figure 5 shows the ROI for each specimen and Table 1 lists the measured lateral load and drift for the peak of each cycle. The ROI's are smaller than the original estimate because of obstructions in the photos that cover some parts of the ROI, which would cause distortion in the analysis results. Nonetheless, the ROI captures a large portion of the surface of the shear wall.

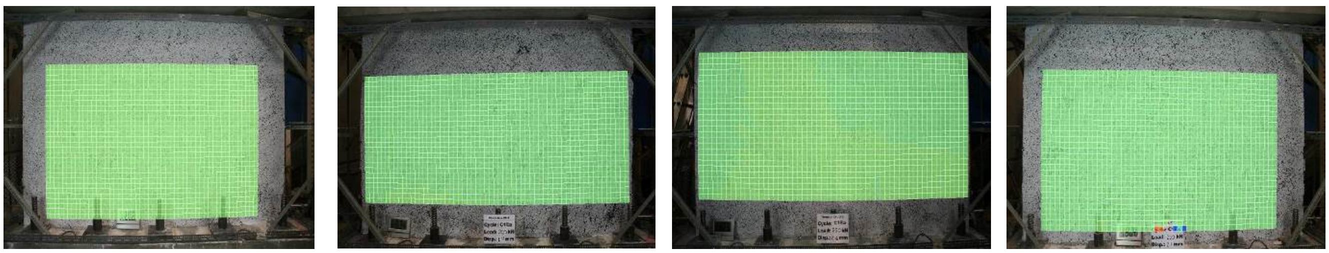

(a) CW1 (b) RW1 (c) CW2 (d) RW2

Fig. 5 – Actual measurement region in each test

Table 1 - Measured lateral load and drift for each peak cycle

| Cycle I.D. | CW1 | | RW1 | | CW2 | | RW2 | |
|---|---|---|---|---|---|---|---|---|
| | **Drift (*mm*)** | **Force (*kN*)** | **Drift (*mm*)** | **Force (*kN*)** | **Drift (*mm*)** | **Force (*kN*)** | **Drift (*mm*)** | **Force (*kN*)** |
| C1Ea | 0.45 | 265 | 1.71 | 226 | 0.618 | 264 | 2.1 | 243 |
| C1Ra | 0.36 | 249 | 0.85 | 221 | 0.29 | 371 | 1.68 | 245 |
| C1Eb | 0.48 | 279 | 1.72 | 218 | 0.601 | 275 | 2.28 | 236 |
| C1Rb | 0.46 | 282 | 0.8 | 214 | 0.54 | 442 | 1.79 | 248 |
| C2Ea | 1.49 | 520 | 3.16 | 392 | 1.55 | 510 | 4.1 | 391 |
| C2Ra | 1.62 | 552 | 1.74 | 412 | 0.9 | 537 | 3.23 | 404 |
| C2Eb | 1.56 | 541 | 3.51 | 420 | 1.71 | 530 | 4.45 | 390 |
| C2Rb | 1.71 | 552 | 1.76 | 412 | 1.09 | 539 | 3.47 | 412 |
| C3Ea | 2.74 | 796 | 5.76 | 746 | 2.75 | 765 | 8.57 | 670 |
| C3Ra | 2.89 | 793 | 3.26 | 759 | 2.19 | 787 | 5.29 | 663 |
| C3Eb | 2.81 | 780 | 5.99 | 765 | 2.83 | 762 | 8.96 | 517 |
| C3Rb | 3.03 | 784 | 3.32 | 760 | 2.43 | 785 | 5.63 | 681 |
| C4Ea | 4.1 | 1060 | 7.44 | 1035 | 4.11 | 1026 | 10.4 | 496 |
| C4Ra | 4.55 | 1050 | 4.37 | 1000 | 3.7 | 1030 | 7.69 | 760 |
| C4Eb | 4.33 | 1060 | 7.64 | 1040 | 4.31 | 1048 | 11 | 295 |
| C4Rb | 4.89 | 1050 | 4.43 | 1000 | 4.12 | 1046 | 8 | 589 |
| C5Ea | 6.15 | 1330 | 8.9 | 1270 | 6.11 | 1238 | 10 | 203 |
| C5Ra | 7 | 1310 | 5.73 | 1260 | 5.54 | 1250 | 9.28 | 539 |
| C5Eb | 6.82 | 1340 | 9.28 | 1295 | 6.28 | 1088 | --- | --- |
| C5Rb | 8.46 | 1330 | 5.92 | 1260 | 6.01 | 1216 | --- | --- |
| C6Ea | --- | --- | 11.71 | 1480 | 7.39 | 1175 | 12.3 | 199 |
| C6Ra | --- | --- | 8 | 1440 | 8.13 | 1273 | 10.3 | 389 |
| C6Eb | --- | --- | 11.6 | 1140 | 8.09 | 981 | --- | --- |
| C6Rb | --- | --- | 7.9 | 1250 | 8.59 | 1117 | --- | --- |
| C7Ea | --- | --- | --- | --- | 9.47 | 1012 | 14.6 | 178 |
| C7Ra | --- | --- | --- | --- | 10.7 | 1110 | 14.8 | 323 |

* Notes: --- denotes the cycle was not carried out, "E" denotes a push cycle, "R" denotes a pull cycle.

In specimens CW1 and CW2, the image analysis technique is used to track the concrete crack progressions throughout the test. In contrast to other image analysis methods that detect cracks in the concrete by observing the formation of dark lines in the images, ImPro Stereo estimates the crack distribution and their opening widths according to the analyzed surface displacement field. This is a superior alternative because the dark line of a crack in the concrete only appears when its opening is as wide as the equivalent width of a pixel in the photo. A crack that is much thinner than a pixel would be difficult to recognize. However, even if a crack is wider than a pixel, the width of that crack cannot be measured precisely because the boundary of the crack in the photo is typically not clear and there would be measurement error equivalent to the width of a pixel. Alternatively, the displacement field approach provides sub-pixel accuracy, typically 0.1 pixels or smaller with adequate image quality. In this study, each pixel measures approximately 0.95mm, making the accuracy of the surface displacement fields as small as 0.1mm. The technical details of the surface displacement, crack field, and strain field estimation methods have been discussed in previous works [2, 3] and are not redundantly discussed here.

Figure 6 shows the crack distributions for selected peaks and their corresponding positions in the cyclic displacement history for specimen CW1. The shade of the crack in the crack fields indicates the relative width of the crack opening. Because of the shear dominant nature of low aspect ratio squat shear walls and the deficiencies in the design of the specimens, a significant number of diagonal shear cracks are observed in the image analysis results. In specimen CW1, results show that the cracks in the "pull" cycles (C1Ra, C2Ra, and so on) occur earlier in the test and are generally wider than those in the "push" cycles (C1Ea, E2Ea, and so on). First diagonal cracking in the push direction does not occur until the second load cycle. Figure 7 narrows the color-map range and demonstrates the presence of the diagonal shear cracks during the first load cycle. The first crack opening widths during the second load cycle are approximately 0.12 mm according to the image analysis results. In the pull cycles, a thin crack, approximately 0.23mm in width is measured during the first load cycle. The measured lateral displacement of the wall during this stage of the test is only 0.36 mm (drift ratio of 0.02%). Using conventional crack measurement techniques these cracks would be very difficult to capture because they would be invisible to the naked eye. Under subsequent load cycles, the image analysis technique captures the opening and closing of diagonal cracks in the concrete and the colour-map shows the widening of the cracks during each cycle. The largest measured crack width during the push cycles is 0.4mm. The maximum diagonal crack width is 1.8mm during the final load cycle in the pull direction after a diagonal tension shear failure plane forms from one corner of the wall to the other. The noise (black/white spotting) in the crack fields in Fig. 6 and

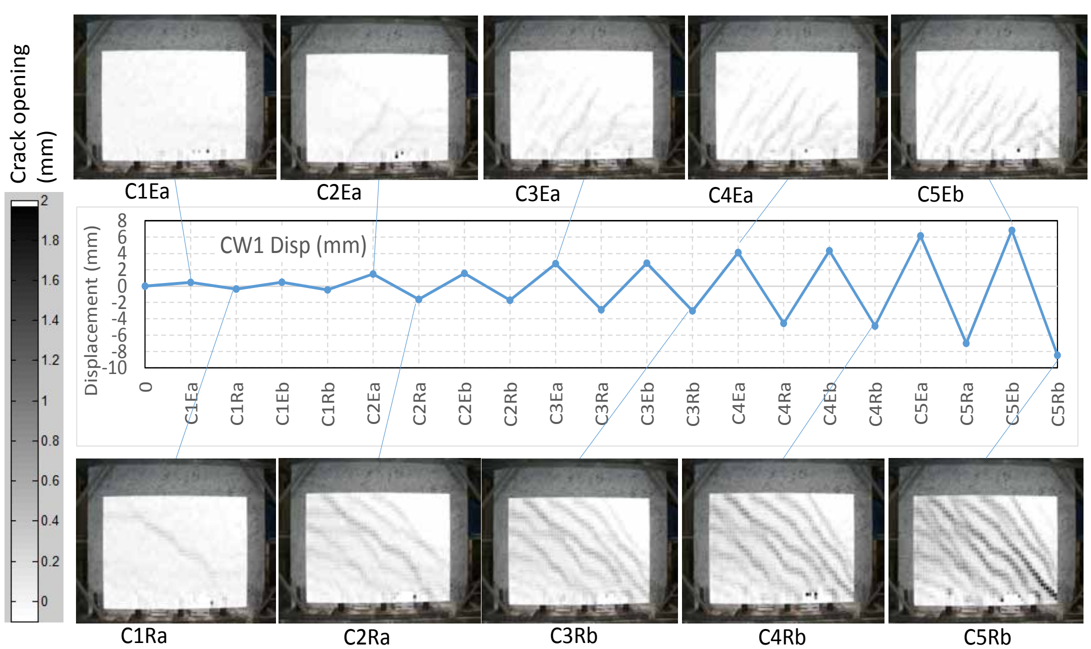


Fig. 6 – Crack distribution fields for specimen CW1 at selected peak cycles

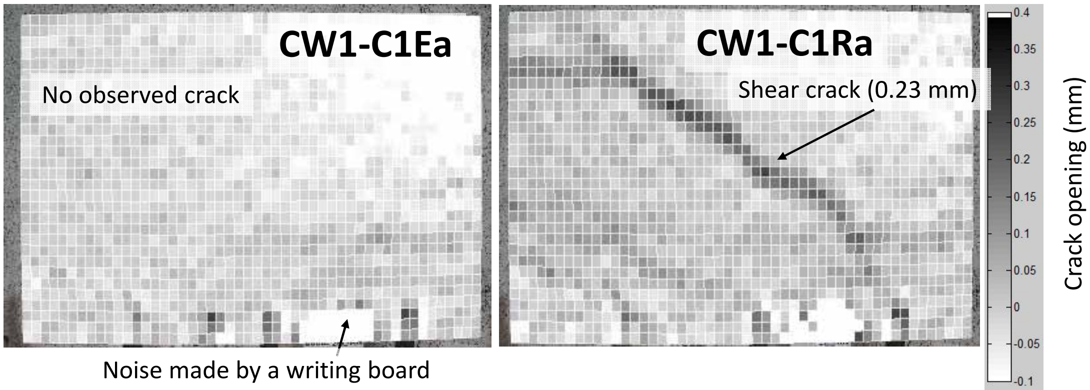


Fig. 7 – Crack distribution fields for specimen CW1 at C1Ea and C1Ra cycles

Fig. 7 are induced by image mismatching during the image analysis procedure, and are caused by object interference in the images. Interfering objects include the post-tensioning rods, moving shadows, and a writing board placed in the image during the peak cycles to denote the maximum load and displacement. These distorted areas do not represent any mechanical phenomenon and can be ignored.

As shown in Fig. 8, the crack distribution for specimen CW2 follows a similar distribution to specimen CW1. However, specimen CW2 is subjected to more loading cycles and larger storey drifts compared to specimen CW1. Once again, diagonal shear cracks in the pull cycles are generally wider and appear earlier than those in the push direction. A very thin 0.1mm shear crack and two horizontal cracks are observed in the first push cycles: 0.1 mm and 0.16 mm wide, respectively. The horizontal cracks in the concrete form at the top of the lap splice, located approximately 420mm above the base of the wall. Although these cracks are not easily identified in the C1Ea subplot in Fig. 8, they can be recognized if the color-map range is narrowed as shown in Fig. 9. This demonstrates the dynamic capabilities of ImPro Stereo to visually analyze experimental results after the experimental test is complete. Results from both tests show that a crack that appears earliest in the test is not

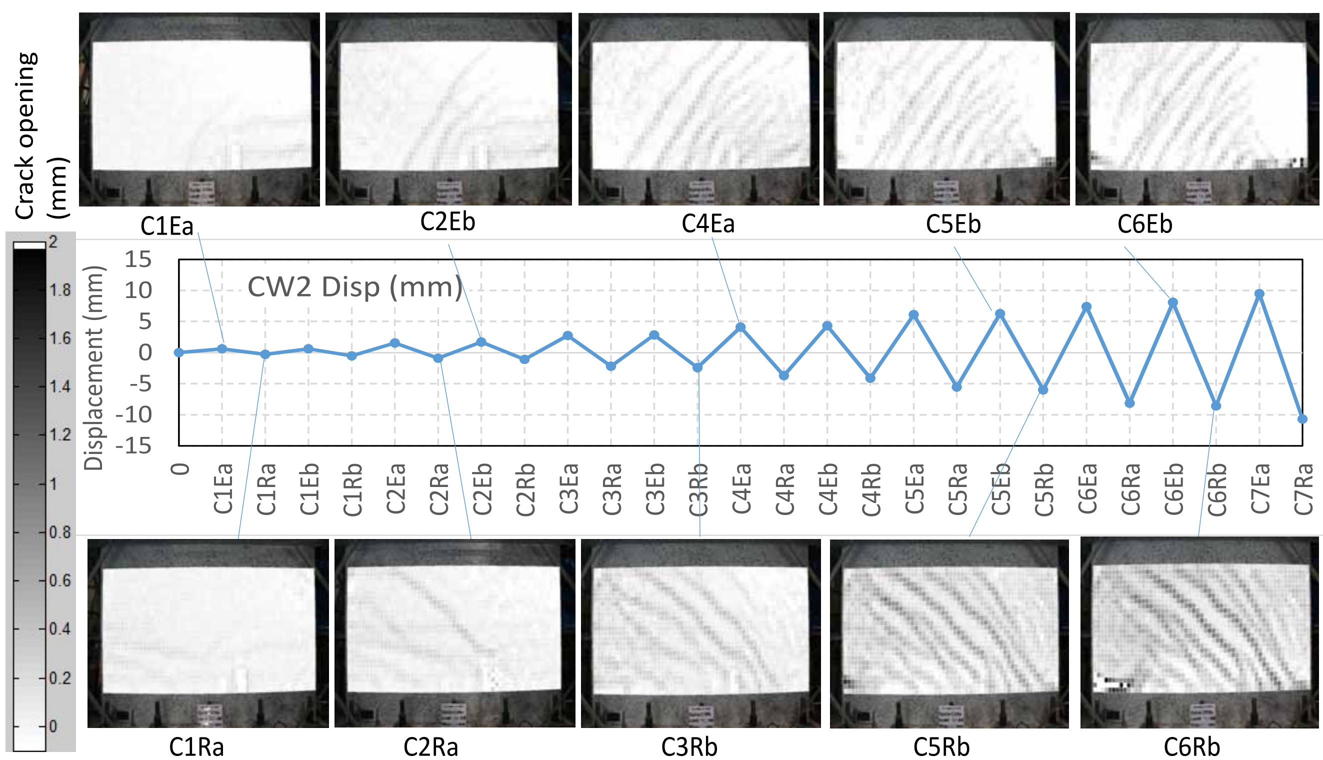


Fig. 8 – Crack distribution fields for specimen CW2 at selected peak cycles

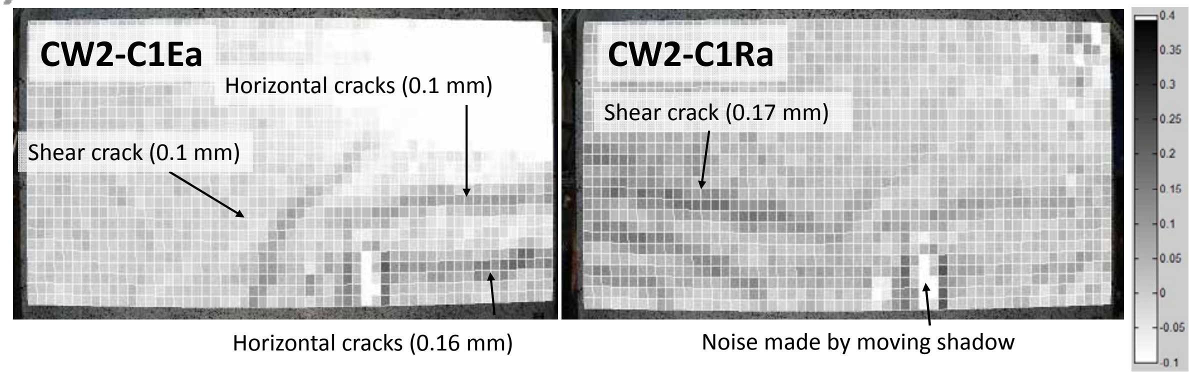


Fig. 9 –Shear crack distribution fields for CW2 at C1Ea and C1Ra cycles

necessarily the widest crack at the end of the test. The thin cracks that appear during the first cycle in specimen CW2 (Fig. 9) did not dilate as much as other diagonal cracks that formed later during the test. Once again, the noise in the lower and middle part of the measurement region are induced by a moving shadow in the measurement region for specimen CW2. Results from the crack distribution analysis demonstrate the capabilities of using ImPro Stereo and the image analysis technique to identify crack distributions and associated crack widths, particularly during the early stages of the test when the identified cracks are not visible to the naked eye.

In contrast with specimens CW1 and CW2, image analysis results for specimens RW1 and RW2 analyze the deformation of the surface of the FRP sheets rather than the surface of the RC wall. The cracks in the original RC wall are covered by the FRP sheets cannot be captured in the photos and cannot be analyzed directly using the image analysis technique discussed in the previous section. As a result, no shear cracks are observed in specimens RW1 or RW2. However, the image analysis technique is able to capture the two-dimensional strain distribution in the FRP sheet throughout the experiment. Figure 10 shows the horizontal shear strain field for specimen RW1 at the peak of selected load cycles. Results show that the strain in the FRP sheet is generally the highest close to the centre of the wall. Theoretically, the strain fields estimated by ImPro Stereo do not capture FRP debonding or separation of the FRP from the concrete substrate because the estimation is based on an assumption that all deformation is in-plane, thus the rectified images are resampled by projecting original photos to a hypothesis plane (with removal of camera lens distortion). However, if debonding did occur, its out-of-plane

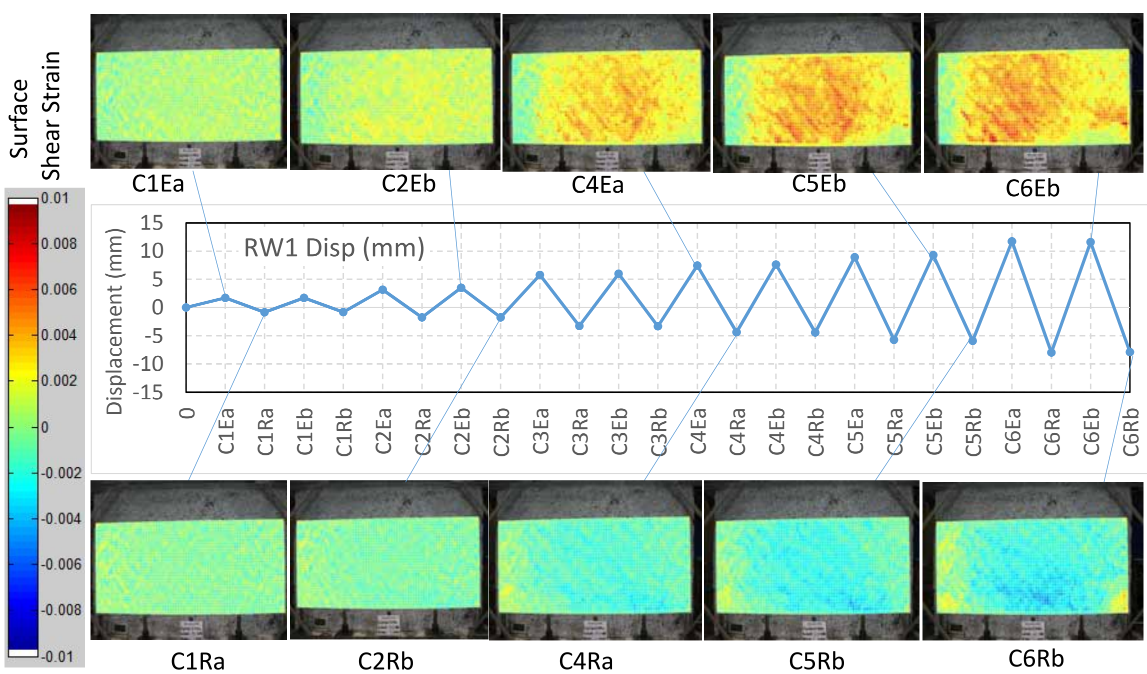


Fig. 10 –Shear strain fields for specimen RW1 at selected peak cycles

movement would lead to incorrect projection and result in large strains with discontinuous strain jumps at the boundary between the bonded and debonded regions. The strain fields shown in Fig. 10 do not show large discontinuities over the surface of the wall, suggesting that debonding either did not occur or was very small. Comparing with observations during the test, some debonding is observed, but it occurs close to the base of the wall outside the ROI so the ability of the image analysis technique to capture debonding in these regions cannot be verified. Nonetheless, ImPro Stereo is shown to be an effective tool to capture the two dimensional shear strain distribution over the entire surface of a structural element, something that is not feasible using conventional electrical strain gauges.

In specimen RW1, two horizontal cracks at the top of the lap splice (720mm from the base of the wall) are captured in the image analysis results. The horizontal crack width can be determined using the $e_{yy}$ (vertical) strain field estimation. Figure 11a shows the $e_{yy}$ strain field for cycle C6Ea, and shows the wide horizontal crack at the right side of the wall. The crack is estimated to be 0.5mm wide using the vertical displacement field. This crack is equivalent to the width of one half of a pixel (as 1 pixel = 0.955 mm in the image analysis of RW1) and as shown in Fig. 11a, the 0.5mm crack is wide enough to present a dark line in the photo. Figure 11b shows a similar horizontal crack at the left side of the wall which forms during the opposite load cycle. Once again, the ability to monitor the surface strain fields and estimate crack widths after the test is already complete is very valuable, especially in earthquake engineering experiments, which may not permit the test to be stopped for an extended period of time to mark and measure crack widths.

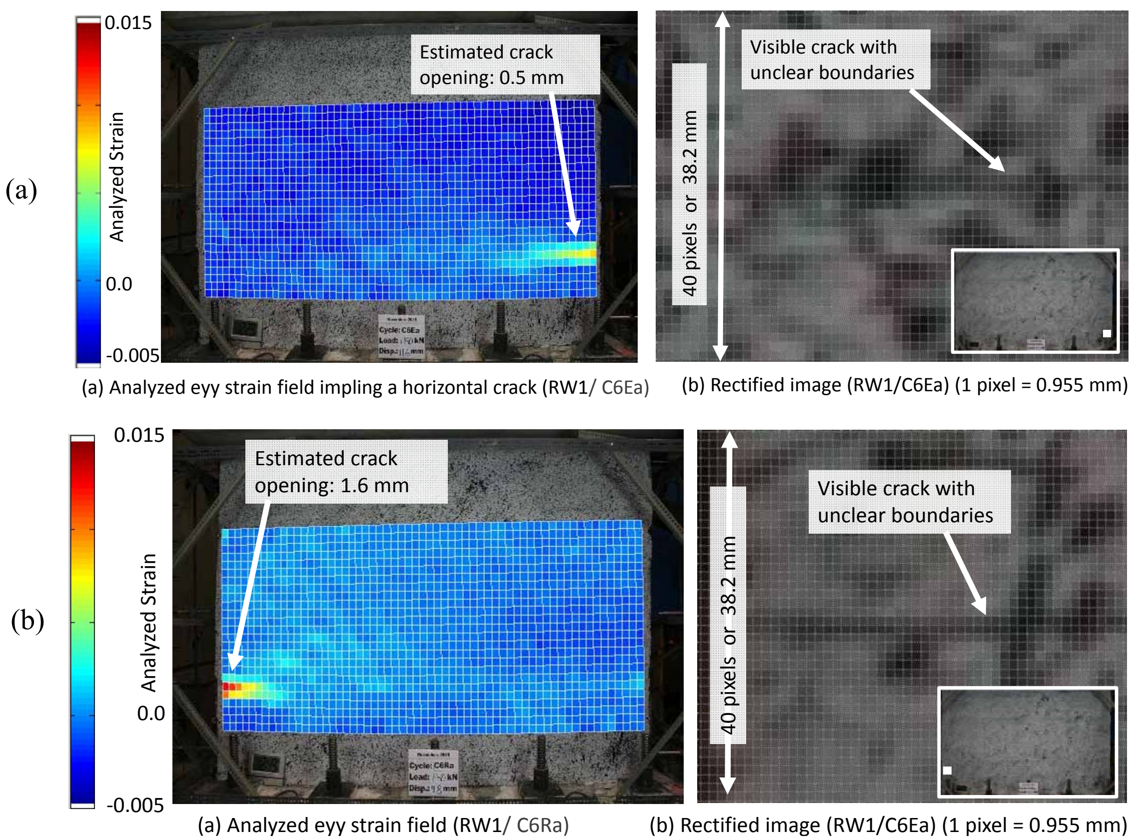


Fig. 11 – Observation of horizontal cracks for RW1 test at: (a) C6Ea cycle; (b) C6Ra cycle

Figure 12 shows the shear strain field for specimen RW2 at selected peak cycles. Results show that in a similar manner to specimen RW1, a wide horizontal crack forms at the height of the lap splice (420mm from the base of the wall). This crack is clearly shown in the shear strain field because there is a relative horizontal slip across the two sides of the crack. Results also show that this slippage occurs in one direction (red line) during the push cycles and subsequently in the other (blue line) during the pull cycles as the shear wall specimen rocks back and forth at the height of the shear plane, which coincides with the top of the lap splice. Figure 13 shows

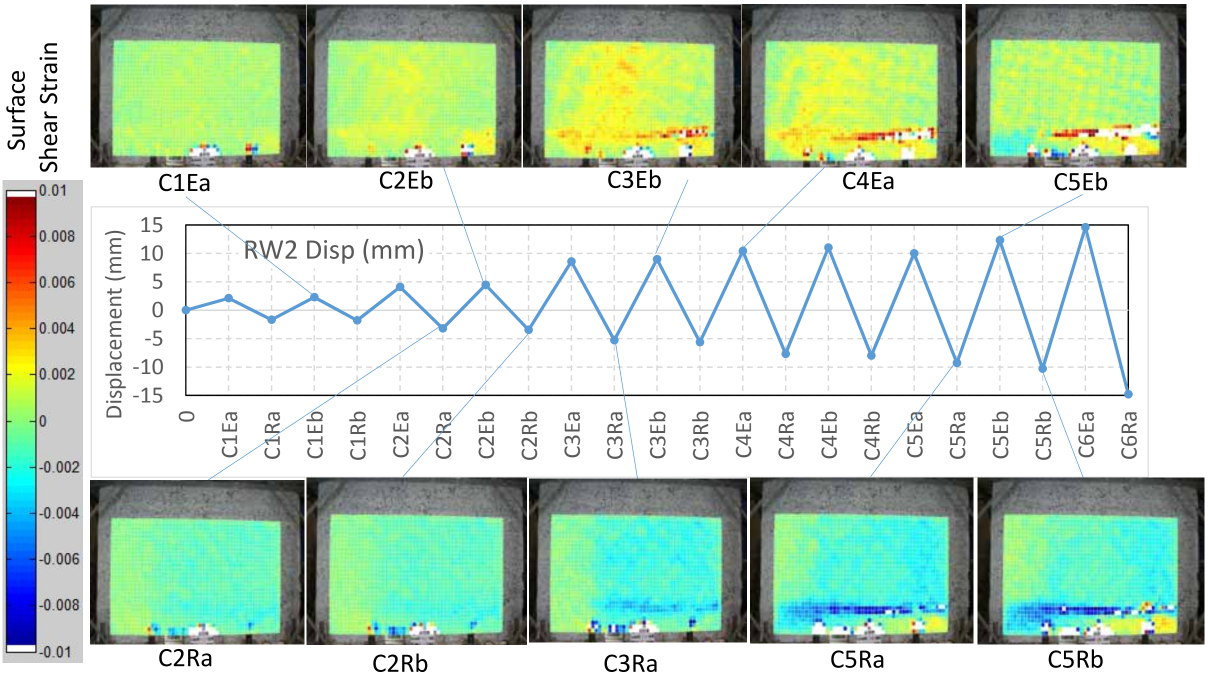


Fig. 12 –Shear strain fields for specimen RW2 at selected peak cycles

the displacement field for the final load cycle, which clearly identifies the location of the shear plane and the large discrepancy in displacement on the two sides of the crack. The results show that the majority of the displacement occurs above the shear plane, which is determined to open to a maximum width of approximately 11.4mm. The relative horizontal slip on either side of the crack can also be estimated using the displacement field results and reaches a maximum of 3.3mm during the final load cycle. Without the use of the image analysis technique the vertical and horizontal slip at the height of the shear plane could not be determined without a priori knowledge of the location in which the slip is going to occur. The use of ImPro Stereo allows the location and magnitude of deformations in critical areas to be studied in more detail after the test is complete.

## 5. Conclusions

This work employed an image analysis technique implemented in the ImPro Stereo tool to estimate the crack distributions and strain fields in the cyclic tests of two RC shear walls before and after FRP retrofit. Before retrofit, the shear crack distribution and their development are presented. Using the image analysis technique, shear cracks as thin as 0.12 mm can be clearly observed, equivalent to only one-eighth the height of a single

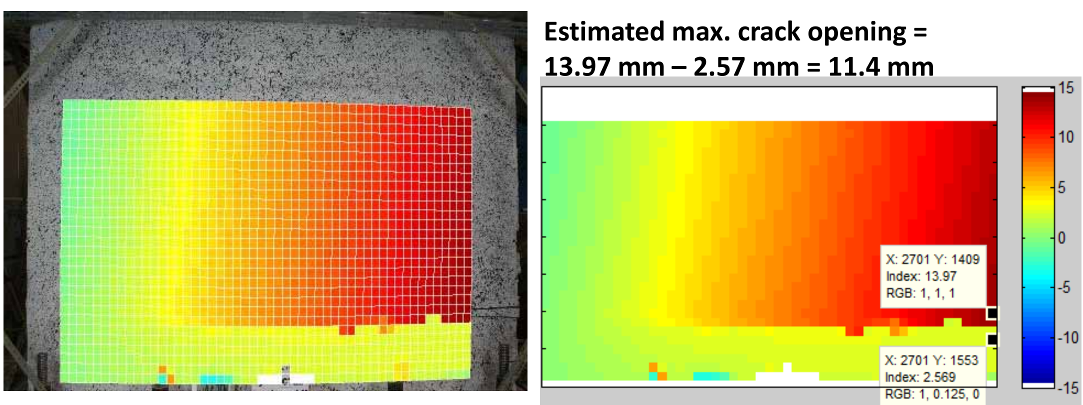


Fig. 13 –Vertical displacement field for RW2 at C6Ea and estimated crack opening

pixel. Cracks of this width would not be visible to the naked eye and would not be detected using the conventional crack marking techniques. In the FRP retrofitted shear wall specimens the crack opening widths are detected as well as the relative horizontal slippage between cracks using the image analyzed displacement fields. The use of the image analysis results can also be employed to estimate the complete two-dimensional strain distribution over the surface of the FRP sheet in the measurement region, something that is not possible using conventional electrical strain gauges. Even though this work did not directly measure the debonding between the FRP sheet and the concrete, the image analysis technique correctly predicted the lack of debonding because no discontinuity in the strain fields is noted, which are typically sensitive to out-of-plane movement. Future studies will aim to use the image analysis method to detect debonding in the laboratory testing of FRP retrofitted RC elements. The use of image analysis and ImPro Stereo allows for crucial information on the behaviour of the structural element to be determined following the test. These results show the versatility of using ImPro Stereo in large scale structural experiments as a simple, safe, and cost effective measurement tool allowing researchers to conduct a detailed step-by-step analysis outside of the laboratory after the test is already complete. The software is shown to be able to accurately capture the crack, displacement and strain fields; information that leads to a better understanding of the behaviour of the structural element and ultimately aids in the development of design expressions and guidelines for use by engineers around the world. This is especially valuable in earthquake engineering experiments, such as shaking table tests or hybrid simulations, when continuous testing is required to replicate realistic earthquake loading scenarios and the test cannot be stopped to take measurements.

## 6. Acknowledgements

The authors gratefully acknowledge the financial support provided by the Canadian Seismic Research Network (CSRN), funded by the Natural Sciences and Engineering Research Council of Canada (NSERC). The technical assistance and material donation provided by Fyfe Co., LLC., Fibrwrap construction is also acknowledge. Image analysis work is financially supported by the Ministry of Science and Technology in Taiwan under project MOST 104-2625-M-027-001.

## 7. References

[1] Yang YS, Chen HM, Lee CS, Jien YH, Hu ZH, Lai WZ (2014): ImPro Stereo. Official site of the ImPro Stereo, Available from: https://sites.google.com/site/improstereoen/.

[2] Yang YS, Huang CW, Wu CL (2012): A simple image-based strain measurement method for measuring the strain fields in an RC-wall experiment. *Journal of Earthquake Engineering and Structural Dynamics*, **41** (1), 1-17.

[3] Yang YS, Yang CM, Huang CW (2015): Thin crack observation in a reinforced concrete bridge pier test using image processing and analysis. *Journal of Advances in Engineering Software,* **83**, 99-108.

[4] Camera Calibration Toolbox for MATLAB (2008): Available from: http://www.vision.caltech.edu/bouguetj/calib_doc/index.html.

[5] Open Source Computer Vision (2016): Available from: http://opencv.org/.

[6] American Concrete Institute (ACI) (1968): Building Requirements for Structural Concrete. *American Concrete Institute ACI 318-68*, Farmington Hills, MI, USA.

[7] Canadian Standards Association (CSA) (1977): Code for the Design of Concrete Structures for Buildings. *Canadian Standards Association CAN3-A23.3-M77,* Rexdale, ON, Canada.

[8] Woods JE, Lau DT, Cruz-Noguez CA (2016): Repair of earthquake damaged squat reinforced concrete shear walls using externally bonded CFRP sheets. *Proceedings of the 16th World Conference on Earthquake Engineering,* Santiago, Chile, 1-12.